Available online at www.sciencedirect.com
ScienceDirect
Journal of Sound and Vibration 303 (2007) 873–894
JOURNAL OF SOUND AND VIBRATION
www.elsevier.com/locate/jsvi

Using the Fourier-series approach to study interactions between moving wheels and a periodically supported rail

X. Sheng[a,*,1], M. Li[a], C.J.C. Jones[b], D.J. Thompson[b]

[a]*Civil Engineering Department, East China Jiaotong University, Nanchang, Jiangxi 330013, China*
[b]*ISVR, University of Southampton, Highfield, Southampton SO17 1BJ, England, UK*

Received 16 March 2006; received in revised form 7 December 2006; accepted 6 February 2007
Available online 23 March 2007

Abstract

In this paper, the Fourier-series approach is employed to study wheel–rail interactions generated by a single, or multiple wheels moving at a constant speed along a railway track. This approach has been previously explored by other researchers and what is presented here is an improved version. In this approach, the track is represented by an infinitely long periodic structure with the period equal to the sleeper spacing and the vertical irregular profile (roughness) of the railhead is assumed to be periodic in the track direction with the period equal to the length of a number (integer), N, of sleeper bays. By assuming linear dynamics for the wheel/track system and for steady state, each wheel/rail force is a periodic function of time and can be expressed as a Fourier series. Fourier coefficients are then shown to be determined by solving, separately, N sets of linear algebraic equations. The coefficient matrix of each set of equations is independent of rail roughness and therefore this approach is particularly useful in modelling the generation and growth of rail roughness of short wavelengths. Excitation purely from the axle loads moving over the periodic track structure is realised by assuming a smooth railhead surface, and subsequently roughness equivalent to such an excitation is defined and evaluated. This equivalent roughness may, in addition to the actual rail roughness, be input into models in which the effect of moving axle loads has been excluded, so that the predictions from those models can be improved. Results are produced using the improved Fourier-series approach to investigate the effects of wheel speeds, roughness wavelengths and interactions between multiple wheels on wheel/rail contact forces.

1. Introduction

Wheel–rail interactions play a key role in the generation of wheel/rail noise, the growth of rail roughness and the formation of rail corrugation. These issues are of high frequencies up to several thousands Hertz. Since frequencies are much higher than the natural frequencies of the primary suspensions, only the unsprung masses of a train need to be considered each with an axle load applied on the mass centre. The most comprehensive and widely employed wheel/rail noise generation models are those developed by Remington

*Corresponding author. Tel.: +44 1484 440522.
E-mail address: shengxiaozhen@hotmail.com (X. Sheng).
[1]Current address: Applied Mechanics Group, Technical Centre, Cummins Turbo Technologies Ltd., St. Andrew's Road, Huddersfield HD1 6RA, England, UK.

0022-460X/$ - see front matter © 2007 Elsevier Ltd. All rights reserved.
doi:10.1016/j.jsv.2007.02.007

[1,2] and Thompson [3,4]. A large number of papers have been published to model short-pitch rail corrugation by e.g. Müller [5], see also [6], following studies by Valdivia [7], Hempelmann [8] and Frederick [9]. While they all consider in the frequency domain only a single wheel interacting with a rough rail, Igeland [10], using a time-domain model, demonstrates the importance of including multiple wheels in the analysis. Dealing with high-frequency problems normally requires analysis to be performed in the frequency domain. Thus, the motion of the wheels is replaced by the motion of a roughness strip in all the aforementioned frequency-domain models, resulting in a linear, time-invariant system. In the real situation, the wheels are travelling along the track and the roughness is stationary. Not only the irregular profile of the railhead produces dynamic wheel–rail forces, the axle loads moving along the periodic track structure also contributes to wheel–rail dynamic interactions. In other words, due to the varying dynamic stiffness of the rail on discrete supports, vibration is still generated in the wheel/track system even wheels move over a perfectly smooth rail. Such a vibration generation mechanism may be termed *the moving axle load excitation*, in contrast to *the roughness excitation*. The wheel moving speed has effects on both of these two excitations. Since wheels are forced to be stationary in the track direction, the 'moving-roughness approach' is able to consider the roughness excitation without including the effect of the wheel speed, but totally excludes the moving axle load excitation. Furthermore, for some roughness wavelengths this approach changes the vibration propagation characteristics of the rail, i.e. it replaces a propagating vibration mode with a non-propagating one, or vice versa [11].

Consideration of wheels moving along a discretely supported rail is normally achieved in the time domain e.g. [10,12] by solving differential equations as an initial-value problem. Time-domain approaches require the track to be truncated into a finite length. To minimise wave reflections from the truncations and to be able to account for high-frequency vibration, the track section must include at least 100 sleepers and the rail must be modelled using either the finite element method [10] or the modal superposition method [12] employing more than 100 modes. If multiple wheels are present covering a rather long distance, the track section must be much longer and in turn much more elements or modes need to be employed for the rail. This would generate a large number of differential equations of time-varying coefficients. It is time consuming to solve these equations, due not only to the large number of equations, but also to the very small time-steps required for high-frequency vibration. For periodic excitations, extra time is also required for achieving the steady-state solution. However, time-domain approaches do have advantages over frequency-domain ones on some aspects, for example the former are able to deal with nonlinearity (e.g. in the wheel/rail contact) and allow more complex configurations (e.g. suspended sleepers).

To overcome shortcomings of the moving roughness approach so that the moving axle load excitation can be included, some researchers suggest a quasi-static approach [13,14] (in these two references, the moving axle load excitation is termed alternatively *the parametric excitation*). According to this approach, the track provides a varying dynamic stiffness as a load moves. In the calculation of the varying stiffness of the track, $x = ct$ (where c is the speed of the moving load) is set into the receptance, $\alpha_p(x, \omega)$, of the rail at the loading point, x, due to a unit *stationary* harmonic load of frequency ω, and then the receptance is inversed to give the time-dependent dynamic stiffness of the track. Based on this time-dependent dynamic stiffness, a time-domain model can be set up. However, it is shown in Ref. [15] that, the ratio of the displacement of the rail at the loading point to a moving harmonic load is significantly different from $\alpha_p(ct, \omega)$ when ω is close to the pinned–pinned frequency of the track. It is also the fact that, like the moving roughness approach, the quasi-static approach may also replace a propagating vibration mode, which is excited by the moving wheels with a non-propagating one, or do the opposite. This will introduce great errors to wheel–wheel interactions which are provided by the rail. It should be acknowledged that the Green function method presented in Ref. [13] may be a good alternative although its usefulness to deal with multiple wheels is to be investigated.

When the track is modelled as an infinite long, linear and periodic structure and the roughness satisfies certain conditions, steady-state wheel/rail forces and the displacements of the wheel/rail contact points are periodic functions of time. They can be expressed using the Fourier series and linear algebraic equations may be set up to evaluate the Fourier coefficients. Such an approach may be termed *the Fourier-series approach*. This is a frequency-domain 'moving wheel approach' and it is obvious that this approach is highly computationally efficient. Implementation of such an approach was initially done by the present authors for a special case in which the rail roughness is periodic with the period equal to the sleeper spacing [16]. That work

formed a part of a project dealing with the initiation and growth of rail roughness of short wavelengths (30–100 mm), in which wheel/rail interactions must be calculated for a great number of times each with a renewed rail profile [17]. Although the amplitude of rail roughness considered is small (therefore a linear wheel/track model can be assumed), it is important for rolling noise generation [1–4]. It should be acknowledged that the Fourier-series approach had been previously explored and employed in a train–track interaction model, as described in Ref. [18]. This approach was also used in Ref. [19] in which vibrations caused by an unbalanced wheel moving along a smooth rail (i.e. no rail roughness) are investigated and in Ref. [20] in which interactions are addressed between an infinite wheel–train (wheels are identical and equally spaced) and a smooth rail track.

In this paper, the Fourier-series approach is adopted and improved to study wheel–rail interactions generated by a single, or multiple wheels moving at a constant speed along a railway track. In this improved version, the vertical irregular profile (roughness) of the railhead is assumed to be periodic in the track direction with the period equal to the length of a number (integer), N, of sleeper bays. A solution is sought in which all the wheel/rail forces and displacements of the wheel/rail contact points are periodic functions of time with the period equal to N time the sleeper passing time. With a special mathematical treatment, the Fourier coefficients of the wheel/rail forces are shown to be determined by solving, separately, N sets of linear algebraic equations. This improvement not only overcomes the problem described in the second paragraph of Section 4 of Ref. [18], but also makes the Fourier-series approach even more efficient. Detailed derivations are presented in Section 2. Conditions are also given in Section 2.7 under which the period solution exists and is unique. Section 3 describes roughness equivalent to the moving axle load excitation. Results produced using this approach are presented in Section 4; firstly, for a single locomotive wheel and then for four such wheels running over a conventional ballasted track at different speeds and excitation frequencies including the case of purely moving axle load excitation. From these results, conclusions are drawn and summarised in Section 5.

This paper is concerned with the determination of the periodic solution only. From time-domain calculations, it can be generally assumed that this periodic solution is asymptotically stable. Nevertheless, instability can happen in some situations, see e.g. [21].

2. The Fourier-series approach to wheel–rail interaction forces

2.1. Track model and governing equations

The wheel/track model is shown in Fig. 1. The rail is modelled as a Timoshenko beam resting on an infinite number of equally spaced supports. The sleeper spacing is denoted by L. Each of the supports consists of a rail pad, which is modelled as a spring with stiffness k_P, and a sleeper which is modelled as a rigid mass m_S resting on a spring of stiffness k_B representing the ballast. From left to right, the supports are numbered as $-\infty, \ldots, -1, 0, 1, \ldots, \infty$. The jth support is located at $x = jL$. There are a number, M, of wheels moving uniformly at speed c along the track in the positive x-direction. At $t = 0$, the x-coordinates of the wheels (from the 1st to the last) are $a_1, a_2, \ldots, a_M$. Bogie frames and car bodies are excluded from the model since frequencies concerned are much higher than the resonance frequencies of the primary suspensions. However, the wheels are coupled through the rail. If the vertical displacement of the rail is denoted by $w_R(x, t)$ (directed

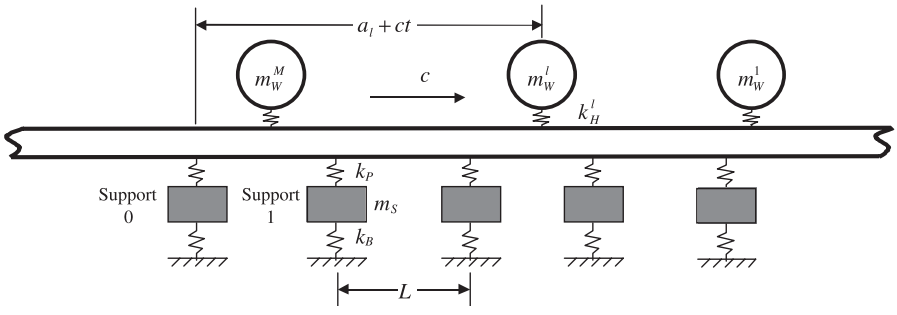

Fig. 1. Wheel/track interaction model.

downwards) and the rotation angle of the cross-section due to the bending moment only is denoted by $\psi_R(x,t)$, then the governing equations for the rail are

$$\rho A\frac{\partial^2 w_R(x,t)}{\partial t^2}-\kappa AG\frac{\partial^2 w_R(x,t)}{\partial x^2}+\kappa AG\frac{\partial \psi_R(x,t)}{\partial x}=\sum_{l=1}^{M}P_l(t)\delta(x-a_l-ct)+\sum_{j=-\infty}^{\infty}F_j(t)\delta(x-jL), \tag{1a}$$

$$\rho I\frac{\partial^2 \psi_R(x,t)}{\partial t^2}-EI\frac{\partial^2 \psi_R(x,t)}{\partial x^2}-\kappa AG\frac{\partial w_R(x,t)}{\partial x}+\kappa AG\psi_R(x,t)=0. \tag{1b}$$

In Eq. (1a), ρ denotes density, E, Young's modulus, G, shear Young's modulus, A the cross-sectional area of the rail, I the second moment of the cross-section, κ the shear coefficient of the cross-section, $\delta(\cdot)$ Dirac-delta, $P_l(t)$ the lth wheel/rail force, and finally, $F_j(t)$ the force applied by the jth support at the rail.

The wheels are modelled as rigid-body vibrating in the vertical direction. If the vertical displacement (directed upwards) of the lth wheel is denoted by $w^l_W(t)$, then the governing equation is given by

$$m^l_W\ddot{w}^l_W(t)=P_l(t)-W_l, \tag{1c}$$

where m^l_W is the mass of the wheel and W_l is half the axle load. Similarly, differential equations of motion can be written for the supports. A contact spring is inserted between each wheel and the rail. It is assumed that the wheels never loss contact with the rail. This requires that for $l=1,2,\ldots,M$,

$$w_R(a_l+ct,t)+w^l_W(t)+\delta^l_0+(P_l(t)-W_l)/k^l_H=z(a_l+ct), \tag{2}$$

where δ^l_0 is the static deformation of the contact spring between the wheel and rail under the static load, W_l, k^l_H is the contact stiffness and $z(x)$ describes the railhead roughness.

The roughness is assumed to be spatially periodic in the track direction with the period equal to the length of a number, N, of sleeper bays, where $N\geqslant 1$ is an integer. In other words, the profile, denoted by $z(x)$, satisfies $z(x+NL)=z(x)$ for any x. This assumption is practically reasonable; especially for short wavelength roughness. With such a roughness, the track structure is still periodic in the x-direction but the period now becomes NL. This allows the existence of a solution in which, wheel displacements, wheel/rail forces and the displacements of the rail at the wheel/rail contact points are all periodic with the (minimum) period equal to NL/c. In other words, have

$$w^l_W(t+NL/c)=w^l_W(t), \tag{3a}$$

$$P_l(t+NL/c)=P_l(t) \tag{3b}$$

and for the rail and the supports, have

$$w_R(x+NL,t+NL/c)=w_R(x,t), \tag{3c}$$

$$\psi_R(x+NL,t+NL/c)=\psi_R(x,t), \tag{3d}$$

$$F_{j+N}(t+NL/c)=F_j(t). \tag{3e}$$

The main purpose of this paper is to find such a solution for the differential equations of the wheel/track system, as detailed in Sections 2.2–2.6.

2.2. Irregular vertical railhead profile

Since the roughness, $z(x)$, satisfies $z(x+NL)=z(x)$ for any x, it can be expressed as a sum of an infinite number of spatial harmonics using Fourier series

$$z(x)=\sum_{n=-\infty}^{\infty}Z_n e^{in(\beta_0/N)x}, \tag{4}$$

where $\mathrm{i}=\sqrt{-1}$, $\beta_0=2\pi/L$, Z_n is a complex number with $Z_0=0$. Owing to the filtering effect of the wheel–rail contact patch [22], only roughness with wavelengths greater than about 0.02 m is important (roughness expressed in Eq. (4) is understood to be the filtered roughness). Therefore, the highest order of the harmonics that should be considered is determined by

$$|n|\leqslant\tfrac{2\pi N}{0.02\beta_0}=30N \tag{5}$$

for $L=0.6$ m. In real calculation, n may be taken to be within the range of $-50N\leqslant n\leqslant 50N$. Since $z(x)$ must be a real function of x, Z_{-n} must be the conjugate of Z_n. Now have,

$$\begin{aligned}
z(x)&=\sum_{n=-\infty}^{\infty}Z_n\mathrm{e}^{\mathrm{i}n(\beta_0/N)x}\\
&=\cdots+\sum_{n=-(3N-1)}^{-(2N+1)}+(-2N)+\sum_{n=-(2N-1)}^{-(N+1)}+(-N)+\sum_{n=-(N-1)}^{-1}+(0)\\
&\quad+\sum_{n=1}^{N-1}+(N)+\sum_{n=N+1}^{2N-1}+(2N)+\cdots\\
&=\sum_{k=-\infty}^{-1}\left(Z_{kN}\mathrm{e}^{\mathrm{i}k\beta_0x}+\sum_{n=kN+1}^{(k+1)N-1}Z_n\mathrm{e}^{\mathrm{i}n(\beta_0/N)x}\right)+\sum_{k=0}^{\infty}\left(Z_{kN}\mathrm{e}^{\mathrm{i}k\beta_0x}+\sum_{n=kN+1}^{(k+1)N-1}Z_n\mathrm{e}^{\mathrm{i}n(\beta_0/N)x}\right)\\
&=\sum_{k=-\infty}^{-1}\left(Z_{kN}\mathrm{e}^{\mathrm{i}k\beta_0x}+\sum_{n'=1}^{N-1}Z_{kN+n'}\mathrm{e}^{\mathrm{i}((kN+n')/N)\beta_0x}\right)+\sum_{k=0}^{\infty}\left(Z_{kN}\mathrm{e}^{\mathrm{i}k\beta_0x}+\sum_{n'=1}^{N-1}Z_{kN+n'}\mathrm{e}^{\mathrm{i}((kN+n')/N)\beta_0x}\right)\\
&=\sum_{k=-\infty}^{-1}\left(Z_{kN}\mathrm{e}^{\mathrm{i}k\beta_0x}+\sum_{n'=1}^{N-1}Z_{kN+n'}\mathrm{e}^{\mathrm{i}k\beta_0x}\,\mathrm{e}^{\mathrm{i}(n'/N)\beta_0x}\right)+\sum_{k=0}^{\infty}\left(Z_{kN}\mathrm{e}^{\mathrm{i}k\beta_0x}+\sum_{n'=1}^{N-1}Z_{kN+n'}\mathrm{e}^{\mathrm{i}k\beta_0x}\mathrm{e}^{\mathrm{i}(n'/N)\beta_0x}\right)\\
&=\sum_{n'=1}^{N-1}\left(\sum_{k=-\infty}^{-1}Z_{kN+n'}\mathrm{e}^{\mathrm{i}k\beta_0x}+\sum_{k=0}^{\infty}Z_{kN+n'}\mathrm{e}^{\mathrm{i}k\beta_0x}\right)\mathrm{e}^{\mathrm{i}(n'/N)\beta_0x}+\sum_{k=-\infty}^{\infty}Z_{kN}\mathrm{e}^{\mathrm{i}k\beta_0x}\\
&=\sum_{n'=0}^{N-1}\left(\sum_{k=-\infty}^{\infty}Z_{kN+n'}\mathrm{e}^{\mathrm{i}k\beta_0x}\right)\mathrm{e}^{\mathrm{i}(n'/N)\beta_0x},
\end{aligned}$$

i.e.

$$z(x)=\sum_{n=0}^{N-1}\left(\sum_{k=-\infty}^{\infty}Z_{kN+n}\mathrm{e}^{\mathrm{i}k\beta_0x}\right)\mathrm{e}^{\mathrm{i}(n/N)\beta_0x}=\sum_{n=0}^{N-1}\left(\sum_{k=-\infty}^{\infty}\tilde{Z}_{nk}\,\mathrm{e}^{\mathrm{i}k\beta_0x}\right)\mathrm{e}^{\mathrm{i}(n/N)\beta_0x}, \tag{6}$$

where

$$\tilde{Z}_{nk}=Z_{kN+n},\quad n=0,1,\ldots,N-1. \tag{7}$$

According to Eqs. (5) and (7), for wheel–rail interaction evaluation, only terms satisfying $|kN+n|\leqslant 30N$ need to be included in the inner series of Eq. (6). This gives $-30-n/N\leqslant k\leqslant 30-n/N$, or $-31\leqslant k\leqslant 30$. In actual calculation, k may be taken to be within the range of $-50\leqslant k\leqslant 50$ in Eq. (6).

For roughness of a single wavelength, $z(x)=A\cos(2\pi x/\lambda)$, where, A is the amplitude and λ the wavelength. When the wavelength is less than the sleeper spacing and L/λ is a rational number, then there exist three positive integers, k, n and N ($n<N$) such that $L/\lambda=k+n/N$. This indicates the profile is a periodic function with the period equal to NL. It can be shown that

$$z(x)=\tfrac{1}{2}A\mathrm{e}^{\mathrm{i}k\beta_0x}\,\mathrm{e}^{\mathrm{i}\beta_0(n/N)x}+\tfrac{1}{2}A\mathrm{e}^{-\mathrm{i}(k+1)\beta_0x}\,\mathrm{e}^{\mathrm{i}\beta_0((N-n)/N)x}, \tag{8}$$

which is a special case of Eq. (6).

2.3. Interaction forces between wheel and rail

According to Eq. (3b), the *compressive* wheel/rail force, $P_l(t)$, between the lth wheel and the rail is periodic of NL/c. Similar to Eq. (6), it may be expressed as

$$P_l(t) = \sum_{n=0}^{N-1} \left(\sum_{k=-\infty}^{\infty} \tilde{P}_{nk}^{l} e^{ik\Omega_0 t} \right) e^{i(n/N)\Omega_0 t}, \tag{9}$$

where $\Omega_0 = (2\pi c/L) = \beta_0 c$ is the sleeper passing (radian) frequency and $\tilde{P}_{nk}^{l}$ is the amplitude of the harmonic component at frequency $(k + n/N)\Omega_0$ of the lth wheel–rail force. Eq. (9) shows that the wheel–rail force spectrum is discrete with the frequency resolution being $\Omega_0/(2\pi N)$ in Hertz. The component corresponding to $n = k = 0$ is the static load, W_l, i.e. $\tilde{P}_{00}^{l} = W_l$. If the period of the roughness is identical to the sleeper spacing (i.e. $N = 1$), then wheel–rail forces have components at the sleeper passing frequency and its multiples only.

2.4. Vertical displacement of wheel

The vertical displacement, *directed upwards*, at the contact point of the lth wheel due to the lth wheel–rail force can be calculated using the receptance of the wheel, i.e.

$$w_W^l(t) = \sum_{n=0}^{N-1} \left(\sum_{k=-\infty}^{\infty} g_{nk}^{l} \tilde{P}_{nk}^{l} e^{ik\Omega_0 t} \right) e^{i(n/N)\Omega_0 t}, \tag{10}$$

where g_{nk}^{l} is the direct receptance of the lth wheel at frequency $(k+n/N)\Omega_0$ and can be computed using the finite element method. In this paper, the wheel is modelled as a rigid-body vibrating in the vertical direction, therefore

$$g_{nk}^{l} = \begin{cases} \text{to be defined} & \text{when } k = n = 0, \\ \frac{1}{-m_W^l[(k+n/N)\Omega_0]^2} & \text{otherwise,} \end{cases} \tag{11}$$

where m_W^l denotes the wheel mass.

2.5. Vertical displacement of rail at wheel/rail contact point

It is well known that (see e.g. [15,23]), under the action of a moving harmonic load and in steady state, the displacement-to-load ratio (the quasi-receptance) of the rail observed from the load is a periodic function of time. The period is equal to the sleeper-passing time. A general formulation is presented in Ref. [15] for the calculation of the Fourier coefficients of this periodic function. According to Ref. [15], the displacement, *directed downwards*, at the lth contact point on the rail due to the jth wheel–rail force is given by

$$w_R^{lj}(t) = \sum_{n=0}^{N-1} \sum_{k=-\infty}^{\infty} \tilde{P}_{nk}^{j} \left(\sum_{m=-\infty}^{\infty} r_m^{lj}((k + n/N)\Omega_0) e^{-im\Omega_0 t} \right) e^{ik\Omega_0 t} e^{i(n/N)\Omega_0 t}, \tag{12}$$

where the sum in the brackets is the time-varying quasi-receptance at the lth contact point due to a unit harmonic force of radian frequency $(k + n/N)\Omega_0$ at the jth contact point, $r_m^{lj}((k + n/N)\Omega_0)$ is the $(-m)$th Fourier coefficient of the quasi-receptance and $\tilde{P}_{nk}^{j}$ is the amplitude of the jth wheel–rail force at frequency $(k + n/N)\Omega_0$ (see Eq. (9)). Eq. (12) can be further manipulated as follows:

$$\begin{aligned} w_R^{lj}(t) &= \sum_{n=0}^{N-1} \sum_{k=-\infty}^{\infty} \tilde{P}_{nk}^{j} \left(\sum_{m=-\infty}^{\infty} r_m^{lj}((k + n/N)\Omega_0) e^{i(k-m)\Omega_0 t} \right) e^{i(n/N)\Omega_0 t} \\ &= \sum_{n=0}^{N-1} \sum_{k=-\infty}^{\infty} \tilde{P}_{nk}^{j} \left(\sum_{m=-\infty}^{\infty} r_{k-m}^{lj}((k + n/N)\Omega_0) e^{im\Omega_0 t} \right) e^{i(n/N)\Omega_0 t} \end{aligned}$$

$$= \sum_{n=0}^{N-1}\sum_{m=-\infty}^{\infty}\left(\sum_{k=-\infty}^{\infty} r_{k-m}^{lj}((k+n/N)\Omega_0)\tilde{P}_{nk}^{j}\right) e^{im\Omega_0 t}\, e^{i(n/N)\Omega_0 t}$$

$$= \sum_{n=0}^{N-1}\sum_{k=-\infty}^{\infty}\left(\sum_{m=-\infty}^{\infty} r_{m-k}^{lj}((m+n/N)\Omega_0)\tilde{P}_{nm}^{j}\right) e^{ik\Omega_0 t}\, e^{i(n/N)\Omega_0 t}. \quad (13)$$

Eq. (13) does show that, the displacements of the wheel/rail contact points are periodic function of time with the period equal to NL/c.

2.6. Determination of wheel–rail force

It is assumed that the wheels are always in contact with the rail via a linearised Hertz contact spring calculated at the static component, W_l, of the wheel–rail force. Since the filtered roughness is used, the stiffness of the contact spring at the lth contact point, k_H^l, can be evaluated based on a smooth rail profile [22]. According to Eq. (2), have

$$w_W^l(t) + \sum_{j=1}^{M} w_R^{lj}(t) + \delta_0^l + (P_l(t) - W_l)/k_H^l = z(a_l + ct), \quad l = 1, 2, \ldots, M, \quad (14)$$

where δ_0^l is the static deformation of the contact spring under the static load, W_l. Note that in Eq. (14), the rail roughness is directed upwards. Inserting Eqs. (6), (9), (10) and (13) into Eq. (14) yields

$$\begin{aligned}
&\sum_{n=0}^{N-1}\left(\sum_{k=-\infty}^{\infty} g_{nk}^l \tilde{P}_{nk}^l e^{ik\Omega_0 t}\right) e^{i(n/N)\Omega_0 t} \\
&\quad + \sum_{j=1}^{M}\left(\sum_{n=0}^{N-1}\sum_{k=-\infty}^{\infty}\left(\sum_{m=-\infty}^{\infty} r_{m-k}^{lj}((m+n/N)\Omega_0)\tilde{P}_{nm}^{j}\right) e^{ik\Omega_0 t}\, e^{i(n/N)\Omega_0 t}\right) \\
&\quad + \tfrac{1}{k_H^l}\sum_{n=0}^{N-1}\sum_{k=-\infty}^{\infty}\tilde{P}_{nk}^l\, e^{ik\Omega_0 t}\, e^{i(n/N)\Omega_0 t} - \frac{1}{k_H^l} W_l \\
&= -\delta_0^l + \sum_{n=0}^{N-1}\sum_{k=-\infty}^{\infty}\tilde{Z}_{nk}\, e^{ik\beta_0(a_l+ct)}\, e^{i(n/N)\beta_0(a_l+ct)}
\end{aligned}$$

or

$$\begin{aligned}
&\sum_{n=0}^{N-1}\left(\sum_{k=-\infty}^{\infty} g_{nk}^l \tilde{P}_{nk}^l e^{ik\Omega_0 t}\right) e^{i(n/N)\Omega_0 t} \\
&\quad + \sum_{n=0}^{N-1}\sum_{k=-\infty}^{\infty}\left(\sum_{m=-\infty}^{\infty}\sum_{j=1}^{M} r_{m-k}^{lj}((m+n/N)\Omega_0)\tilde{P}_{nm}^{j}\right) e^{ik\Omega_0 t}\, e^{i(n/N)\Omega_0 t} \\
&\quad + \frac{1}{k_H^l}\sum_{n=0}^{N-1}\sum_{k=-\infty}^{\infty}\tilde{P}_{nk}^l\, e^{ik\Omega_0 t}\, e^{i(n/N)\Omega_0 t} - \frac{1}{k_H^l} W_l \\
&\quad = -\delta_0^l + \sum_{n=0}^{N-1}\sum_{k=-\infty}^{\infty}\tilde{Z}_{nk} e^{ik\beta_0 a_l}\, e^{i(n/N)\beta_0 a_l}\, e^{ik\Omega_0 t}\, e^{i(n/N)\Omega_0 t}, \quad (15)
\end{aligned}$$

since $\Omega_0 = \beta_0 c$.

For any combination of n and k except for $n = k = 0$, Eq. (15) gives

$$\left(g_{nk}^l + 1/k_H^l\right)\tilde{P}_{nk}^l + \sum_{m=-\infty}^{\infty}\sum_{j=1}^{M} r_{m-k}^{lj}((m+n/N)\Omega_0)\tilde{P}_{nm}^{j} = \tilde{Z}_{nk}\, e^{ik\beta_0 a_l}\, e^{i(n/N)\beta_0 a_l}. \quad (16)$$

Especially when $n = 0$ and $k \neq 0$

$$\left(g_{0k}^{l} + 1/k_H^{l}\right)\tilde{P}_{0k}^{l} + \sum_{\substack{m=-\infty \\ m\neq 0}}^{\infty}\sum_{j=1}^{M} r_{m-k}^{lj}(m\Omega_0)\tilde{P}_{0m}^{j} = \tilde{Z}_{0k}\mathrm{e}^{\mathrm{i}k\beta_0 a_l} - \sum_{j=1}^{M} r_{-k}^{lj}(0\Omega_0)W_j, \tag{17}$$

since $\tilde{P}_{00}^{j} = W_j$.

For $n = k = 0$, Eq. (15) gives

$$g_{00}^{l} W_l + \sum_{m=-\infty}^{\infty}\sum_{j=1}^{M} r_{m}^{lj}(m\Omega_0)\tilde{P}_{0m}^{j} = -\delta_0^{l}. \tag{18}$$

Now unknowns, $\tilde{P}_{0k}^{l}$, where $l = 1, 2, \ldots, M$ and $k = \pm 1, \pm 2, \ldots$, can be determined from Eq. (17). For every $n \neq 0$, unknowns $\tilde{P}_{nk}^{l}$, where $l = 1, 2, \ldots, M$ and $k = 0, \pm 1, \pm 2, \ldots$ can be determined using Eq. (16). Eq. (18) gives the average displacement of the lth wheel

$$w_{W0}^{l} = g_{00}^{l} W_l = -\sum_{m=-\infty}^{\infty}\sum_{j=1}^{M} r_{m}^{lj}(m\Omega_0)\tilde{P}_{0m}^{j} - \delta_0^{l}, \quad l = 1, 2, \ldots, M. \tag{19}$$

Eqs. (16) and (17) contain an infinite number of unknowns. In actual calculation, only a finite number of unknowns, $\tilde{P}_{nk}^{l}$, where, $l = 1, 2, \ldots, M$, $n = 0, 1, \ldots, N-1$ and $k = -K, \ldots, K$ (K is an positive integer. As has been identified in Section 2.2, K may be chosen to be 50), are determined through the following equations:

$$\begin{aligned}\left(g_{0k}^{l} + 1/k_H^{l}\right)\tilde{P}_{0k}^{l} + \sum_{\substack{m=-K \\ m\neq 0}}^{K}\sum_{j=1}^{M} r_{m-k}^{lj}(m\Omega_0)\tilde{P}_{0m}^{j} \\ = \tilde{Z}_{0k}\,\mathrm{e}^{\mathrm{i}k\beta_0 a_l} - \sum_{j=1}^{M} r_{-k}^{lj}(0\Omega_0)W_j, \quad k \neq 0,\end{aligned} \tag{20}$$

$$\left(g_{nk}^{l} + 1/k_H^{l}\right)\tilde{P}_{nk}^{l} + \sum_{m=-K}^{K}\sum_{j=1}^{M} r_{m-k}^{lj}((m + n/N)\Omega_0)\tilde{P}_{nm}^{j} = \tilde{Z}_{nk}\,\mathrm{e}^{\mathrm{i}k\beta_0 a_l}\,\mathrm{e}^{\mathrm{i}(n/N)\beta_0 a_l}, \quad n \neq 0. \tag{21}$$

Eq. (20) may be written in a more compact form

$$[\mathbf{B}]_{0k}\{\tilde{P}\}_{0k} + \sum_{\substack{m=-K \\ m\neq 0}}^{K}[\mathbf{C}]_{0km}\{\tilde{P}\}_{0m} = \{\tilde{Z}\}_{0k} - [\mathbf{C}]_{0k0}\{W\}, \quad k = -K, \ldots, K,\ k \neq 0, \tag{22}$$

where the vectors and matrices are defined as follows:

$$\left\{\tilde{P}\right\}_{0k} = \left(\tilde{P}_{0k}^{1}, \tilde{P}_{0k}^{2}, \ldots, \tilde{P}_{0k}^{M}\right)^{\mathrm{T}} \tag{23a}$$

is a vector consisting of wheel–rail force components at frequency $k\Omega_0$,

$$[\mathbf{B}]_{0k} = \begin{bmatrix} g_{0k}^{1} + 1/k_H^{1} & \cdots & 0 \\ \vdots & \cdots & \vdots \\ 0 & \cdots & g_{0k}^{M} + 1/k_H^{M} \end{bmatrix}, \tag{23b}$$

$$[\mathbf{C}]_{0km} = \begin{bmatrix} r_{m-k}^{11}(m\Omega_0) & \cdots & r_{m-k}^{1M}(m\Omega_0) \\ \vdots & \vdots & \vdots \\ r_{m-k}^{M1}(m\Omega_0) & \cdots & r_{m-k}^{MM}(m\Omega_0) \end{bmatrix}, \tag{23c}$$

$$[\mathbf{C}]_{0k0} = \begin{bmatrix} r^{11}_{m-k}(0\Omega_0) & \cdots & r^{1M}_{m-k}(0\Omega_0) \\ \vdots & \vdots & \vdots \\ r^{M1}_{m-k}(0\Omega_0) & \cdots & r^{MM}_{m-k}(0\Omega_0) \end{bmatrix}, \tag{23d}$$

$$\{\tilde{Z}\}_{0k} = \tilde{Z}_{0k}\left(\mathrm{e}^{\mathrm{i}k\beta_0 a_1}, \ldots, \mathrm{e}^{\mathrm{i}k\beta_0 a_M}\right)^{\mathrm{T}}, \tag{23e}$$

$$\{W\} = (W_1, \ldots, W_M)^{\mathrm{T}}. \tag{23f}$$

From Eq. (22) unknowns, $\tilde{P}^l_{0k}$ ($l = 1, 2, \ldots, M$, $k = -K, \ldots, K$, $k \neq 0$) can be determined.

Similarly, Eq. (21) may be written as

$$[\mathbf{B}]_{nk}\{\tilde{P}\}_{nk} + \sum_{m=-K}^{K} [\mathbf{C}]_{nkm}\{\tilde{P}\}_{nm} = \{\tilde{Z}\}_{nk}, \quad n \neq 0,\ k = -K, \ldots, K, \tag{24}$$

where the vectors and matrices are defined as follows:

$$\left\{\tilde{P}\right\}_{nk} = \left(\tilde{P}^1_{nk}, \tilde{P}^2_{nk}, \ldots, \tilde{P}^M_{nk}\right)^{\mathrm{T}}, \tag{25a}$$

$$[\mathbf{B}]_{nk} = \begin{bmatrix} g^1_{nk} + 1/k^1_H & \cdots & 0 \\ \vdots & \ldots & \vdots \\ 0 & \cdots & g^M_{nk} + 1/k^M_H \end{bmatrix}, \tag{25b}$$

$$[\mathbf{C}]_{nkm} = \begin{bmatrix} r^{11}_{m-k}((m+n/N)\Omega_0) & \cdots & r^{1M}_{m-k}((m+n/N)\Omega_0) \\ \vdots & \vdots & \vdots \\ r^{M1}_{m-k}((m+n/N)\Omega_0) & \cdots & r^{MM}_{m-k}((m+n/N)\Omega_0) \end{bmatrix}, \tag{25c}$$

$$\left\{\tilde{Z}\right\}_{nk} = \tilde{Z}_{nk}\left(\mathrm{e}^{\mathrm{i}k\beta_0 a_1}\,\mathrm{e}^{\mathrm{i}(n/N)\beta_0 a_1}, \ldots, \mathrm{e}^{\mathrm{i}k\beta_0 a_M}\,\mathrm{e}^{\mathrm{i}(n/N)\beta_0 a_M}\right)^{\mathrm{T}}. \tag{25d}$$

From Eq. (22) unknowns, $\tilde{P}^l_{nk}$ ($l = 1, 2, \ldots, M$, $k = -K, \ldots, K$) can be determined for every n, where $n = 1, 2, \ldots, N-1$.

2.7. Existence and uniqueness of periodic wheel/rail fore

Eqs. (20) and (21) have been established for the periodic solution of wheel/rail forces with the period being NL/c. The track structure with the roughness may be thought to have periods of $2NL$, $3NL$ etc and periodic solutions with periods $2NL/c$, $3NL/c$ etc may also be possible. It is now assumed that there exits a periodic solution with the period being $\mu NL/c$, where $\mu > 1$ is an integer. In other words, the lth wheel/rail force can be expressed as

$$P_l(t) = \sum_{n=0}^{\mu N-1} \left(\sum_{k=-\infty}^{\infty} \tilde{P}^l_{nk} \mathrm{e}^{\mathrm{i}k\Omega_0 t} \right) \mathrm{e}^{\mathrm{i}(n/\mu N)\Omega_0 t}. \tag{26}$$

Following the same procedure detailed in Sections 2.2–2.6, it can be shown that the harmonic component amplitude, $\tilde{P}^l_{nk}$, at frequency $(k + n/\mu N)\Omega_0$ is governed by

$$\left(g^l_{0k} + 1/k^l_H\right)\tilde{P}^l_{0k} + \sum_{\substack{m=-K \\ m\neq 0}}^{K} \sum_{j=1}^{M} r^{lj}_{m-k}(m\Omega_0)\tilde{P}^j_{0m}$$

$$= \tilde{Z}_{0k} e^{ik\beta_0 a_l} - \sum_{j=1}^{M} r_{-k}^{lj}(0\Omega_0) W_j, \quad k = -K, \ldots, -1, 1, \ldots, K \tag{27}$$

and

$$\left(g_{nk}^l + 1/k_H^l\right)\tilde{P}_{nk}^l + \sum_{m=-K}^{K}\sum_{j=1}^{M} r_{m-k}^{lj}((m + n/\mu N)\Omega_0)\tilde{P}_{nm}^j = \tilde{Z}_{nk} e^{ik\beta_0 a_l} e^{i(n/\mu N)\beta_0 a_l},$$
$$k = -K, \ldots, -1, 0, 1, \ldots, K, \tag{28}$$

where $n = 1, 2, \ldots, \mu N-1$, therefore $n/\mu N < 1$. Note that, g_{nk}^l is the direct receptance of the lth wheel at frequency $(k + n/\mu N)\Omega_0$ and $\tilde{Z}_{nk}$ is the amplitude of the roughness at wavenumber $(k + n/\mu N)\beta_0$. Since the period of the roughness is NL, and according to Eq. (6), it must have

$$\tilde{Z}_{nk} = 0 \quad \text{when } n \neq 0, \mu, 2\mu, \ldots, \mu(N-1). \tag{29}$$

Thus, when $n \neq \mu, 2\mu, \ldots, \mu(N-1)$, Eq. (28) becomes

$$\left(g_{nk}^l + 1/k_H^l\right)\tilde{P}_{nk}^l + \sum_{m=-K}^{K}\sum_{j=1}^{M} r_{m-k}^{lj}((m + n/\mu N)\Omega_0)\tilde{P}_{nm}^j = 0, \quad k = -K, \ldots, -1, 0, 1, \ldots, K. \tag{30}$$

If coefficient matrix of Eq. (27) is regular and it is also true for the coefficient matrix of Eq. (28) with every n, where $n = 1, 2, \ldots, \mu N-1$, then a unique solution for $\tilde{P}_{nk}^j$ exists and can be worked out from these equations. Especially from Eq. (30),

$$\tilde{P}_{nk}^j = 0, \tag{31}$$

where $j = 1, 2, \ldots, M$, $n \neq 0, \mu, 2\mu, \ldots, \mu(N-1)$ and $k = -K, \ldots, -1, 0, 1, \ldots, K$. This combined with Eq. (26) shows that the wheel/rail forces are periodic with the period being NL/c, rather than $\mu NL/c$.

Now it can be concluded that, if for any real number σ, $0 \leqslant \sigma < 1$, the coefficient matrix of the following equations (unknowns are denoted by X_k^l),

$$\left(g_k^l + 1/k_H^l\right)X_k^l + \sum_{m=-K}^{K}\sum_{j=1}^{M} r_{m-k}^{lj}((m + \sigma)\Omega_0)X_m^j = 0, \tag{32}$$

where $l = 1, 2, \ldots, M$, $k = -K, \ldots, -1, 0, 1 \ldots, K$ and g_k^l is the direct receptance of the lth wheel at frequency $(k+\sigma)\Omega_0$, is regular, then (a) there exists a unique periodic solution for the wheel/rail forces with the smallest period being NL/c; (b) periodic solutions cannot exist to have the smallest period of $2NL/c$, $3NL/c$, etc.

The above condition can be easily verified and is found to hold for all the cases studied in Section 4.

3. Moving axle load excitation and equivalent roughness

Eq. (20) shows that at each (e.g. the lth) wheel there are two excitation mechanisms, the roughness excitation defined by $\tilde{Z}_{0k} e^{ik\beta_0 a_l}$ and the moving axle load excitation given by $-\sum_{j=1}^{M} r_{-k}^{lj}(0\Omega_0)W_j$. The latter depends on the wheel speed, the static loads and the track dynamics. It is the position-varying displacement of the rail at a wheel under the action of the moving static load that causes such an excitation, which in turn excites the wheel/track system into vibration. The greater the static (axle load), the stronger is the moving axle load excitation. If the rail is continuously supported, then the moving axle loads will not generate dynamic wheel/rail forces. In this situation, vibration is expected only for the track structure, not for the wheels. It is seen that Eq. (21) contains roughness excitation only.

According to Eq. (20), the kth component of an equivalent roughness at the lth wheel may be defined as

$$\tilde{Z}_{0k}^l = -e^{-ik\beta_0 a_l}\sum_{j=1}^{M} r_{-k}^{lj}(0\Omega_0)W_j, \quad k = -K, \ldots, K, \; k \neq 0, \tag{33a}$$

$$\tilde{Z}_{00}^{l} = 0 \tag{33b}$$

and this equivalent roughness can be constructed by summing all its components (see Eq. (6))

$$z^{l}(x) = \sum_{k=-K}^{K} \tilde{Z}_{0k}^{l} \, \mathrm{e}^{\mathrm{i}k\beta_0 x} = -\sum_{k=-K}^{K} \left(\sum_{j=1}^{M} r_{-k}^{lj}(0\Omega_0) W_j \right) \mathrm{e}^{\mathrm{i}k\beta_0 (x-a_l)}. \tag{34}$$

It is seen from Eq. (34) that the equivalent roughness is a periodic function of x with the period equal to the sleeper spacing, L, and at different wheels the equivalent roughness may be different not only in phase but also in magnitude. The equivalent roughness is contributed not only by the static load of the 'home' wheel, but also by those of other wheels. The equivalent roughness may be input into a 'moving roughness model' so that predictions from such a model can be improved.

4. Results

In this section, results are produced using the approach derived above for a single locomotive wheel and for four such wheels moving over a conventional ballasted track with UIC60 rails (Fig. 1). Each wheel is modelled as a rigid body having mass 1350 kg and radius 0.575 m. The static load applied by a wheel is evaluated to be 100 kN, half the axle load of the locomotive. The stiffness of the wheel–rail contact spring is calculated to be 1.4×10^9 N/m. A set of typical parameters for the track structure is listed in Table 1. These parameters are for half the structure (i.e. a single rail on half-sleepers) and correspond to a track with concrete monobloc sleepers and moderately stiff rail pads. Results include roughness levels equivalent to the moving axle load excitation, wheel–rail force spectra and wheel–rail force 'position-histories' (i.e. time history plotted against spatial coordinates). The wheel–rail force spectra are discrete; however, they are plotted as if they were continuous.

4.1. Roughness equivalent to moving axle load excitation

Components of roughness equivalent to the moving axle load excitation are calculated according to Eq. (33), and shown in levels in Fig. 2 for a single wheel moving at 20, 40 and 80 m/s along the track. Note that the equivalent roughness displays discrete wavelengths equal to the sleeper spacing, half the spacing, one-third, etc. At wavelengths of 0.3 and 0.6 m, roughness levels are greater than 0 dB and even can be as high as more than 10 dB, comparable to some actual roughness present on main railway lines. This demonstrates the importance of including the moving axle load excitation in wheel–rail interaction problems. For wavelengths less than one-third (0.2 m) of the sleeper spacing, roughness levels follow a linear relationship with wavelengths. The levels for the first two speeds are indistinguishable and for the highest speed the roughness level is increased by about 3 dB only at wavelength 0.3 m, half the sleeper spacing. This is because the combination of the wavelength and speed gives a frequency (266 Hz) near, which the track has a dip

Table 1
Parameters for the vertical dynamics of a track

Density of the rail	$\rho = 7850\,\mathrm{kg/m^3}$
Young's modulus of the rail	$E = 2.1 \times 10^{11}\,\mathrm{N/m^2}$
Shear modulus of the rail	$G = 0.81 \times 10^{11}\,\mathrm{N/m^2}$
Loss factor of the rail	$\eta_R = 0.01$
Cross-sectional area of the rail	$A = 7.69 \times 10^{-3}\,\mathrm{m^2}$
Second moment of area of the rail cross-section	$I = 30.55 \times 10\,\mathrm{m^4}$
Shear coefficient of the rail cross-section	$\kappa = 0.4$
Vertical rail pad stiffness	$k_P = 3.5 \times 10^8\,\mathrm{N/m}$
Rail pad loss factor	$\eta_P = 0.25$
Mass of sleeper	$m_S = 162\,\mathrm{kg}$
Sleeper spacing	$l = 0.6\,\mathrm{m}$
Vertical ballast stiffness	$k_B = 50 \times 10^6\,\mathrm{N/m}$
Loss factor of ballast	$\eta_B = 1.0$

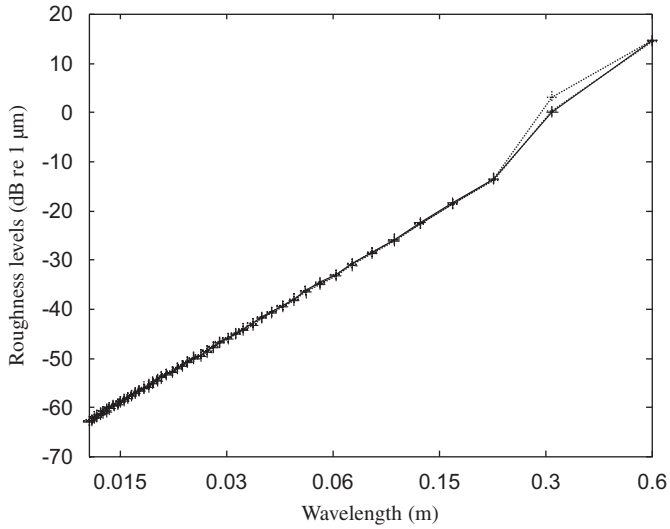

Fig. 2. Roughness levels equivalent to the moving axle load excitation of the wheel moving at 20 m/s (———), 40 m/s (– – –) and 80 m/s (. . . . . .).

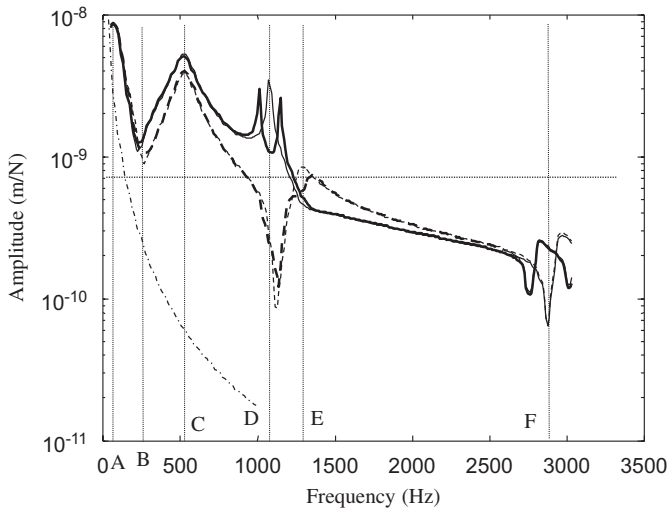

Fig. 3. Displacement-to-force ratio at the loading point due to a stationary or moving (80 m/s) load of different frequencies. ———, stationary load at mid-span; – – –, stationary load above a sleeper; ———, moving load which passes the mid-span at time $t = 0$; – – –, moving load which passes a sleeper at $t = 0$; . . . . . ., receptance of the contact spring; – · –, receptance of the wheel; vertical lines indicating peak or dip frequencies.

receptance (a peak stiffness) (B in Fig. 3). Nevertheless, for wheel–rail noise problem at current operational train speeds, the equivalent roughness may be approximated to be independent of train speed.

The equivalent roughness levels may be used as a lower limit for roughness management. In other words, it is meaningless to require rail roughness to be lower than the equivalent roughness.

4.2. Wheel–rail force: a single wheel moving along the rail

4.2.1. Rail with a smooth railhead

In this sub-section, wheel–rail force is produced for a single wheel moving along the rail with a smooth railhead. The results are shown in Figs. 4 (spectrum) and 5 (time-history). For a smooth railhead, only Eq. (22)

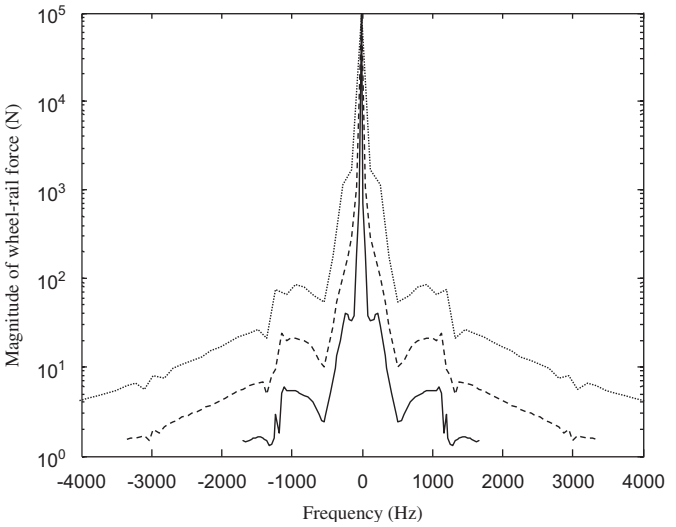

Fig. 4. Wheel–rail force spectrum for the wheel moving at 20 m/s (———), 40 m/s (– – –) and 80 m/s (. . . . . .) over the rail with a smooth railhead.

needs to be solved. It is seen from Fig. 4 that the wheel–rail force spectrum shows a broad peak around the first pinned–pinned frequency (D in Fig. 3, about 1070 Hz), although at this frequency the rail can present a dip or peak receptance depending on the location on the rail. The magnitude of this peak, however, is much less than the component at the sleeper-passing frequency (67 Hz at 40 m/s), even at very high speeds. A dip is observed at about 500 Hz which is caused by the low stiffness (high receptance) of the rail (C in Fig. 3). All the dynamic wheel–rail force components increase as the wheel speed increases. Table 2 shows the ratios of the first three components of the dynamic wheel–rail force to the static load. At speeds below 40 m/s, the component at the sleeper-passing frequency is dominant. However, for higher wheel speeds, the second component at twice the sleeper-passing frequency can be as strong as the first one. This is because the frequency of the second component is within the frequency range (200–300 Hz) within which the rail receptance is minimum (B in Fig. 3). As has identified in Section 2, the wheel–rail force is a spatially periodic function with the period equal to the sleeper spacing. Fig. 5 shows the wheel–rail force variation within a sleeper bay. It can be seen that the maximum wheel–rail force does not necessarily occurs at a sleeper.

4.2.2. Rail with a spatially harmonic railhead

In this case, the roughness is set to be of a single wavelength and the amplitude is chosen to be 10 μm (17 dB re 1 μm), i.e. $z(x) = 1 \times 10^{-5} \cos(2\pi/\lambda)x = 1 \times 10^{-5} \cos(2\pi f/c)x$ (m), where $x = 0$ is chosen to be at a sleeper, f denotes the roughness excitation frequency, c denotes the wheel speed and λ the wavelength. Using Eq. (8), the roughness is transformed to the required form (see Table 3). If the wavelength is a fraction of the sleeper spacing, then $N = 1$ in Eq. (3) and only Eq. (22) needs to be solved. Since the roughness level is much higher than the roughness level equivalent to the moving axle load excitation (see Fig. 2), contributions to the wheel–rail force from the moving axle load excitation are negligible.

For roughness excitation frequencies of 500, 1000 and 2000 Hz, the spectra of the wheel–rail force are shown in Figs. 6–8. It can be seen that, in addition to the peaks at 0 Hz (static load) and the first pinned–pinned frequency, the wheel–rail force spectra have a peak at the roughness excitation frequency. This peak becomes broad when the excitation frequency is near the first pinned–pinned frequency. The magnitude of the component at the roughness excitation frequency is almost independent of the wheel speed, although the magnitudes of other harmonic components increase with the wheel speed. For a thorough understanding, the component at the excitation frequency is calculated for a range of roughness excitation frequencies, as shown in Fig. 9.

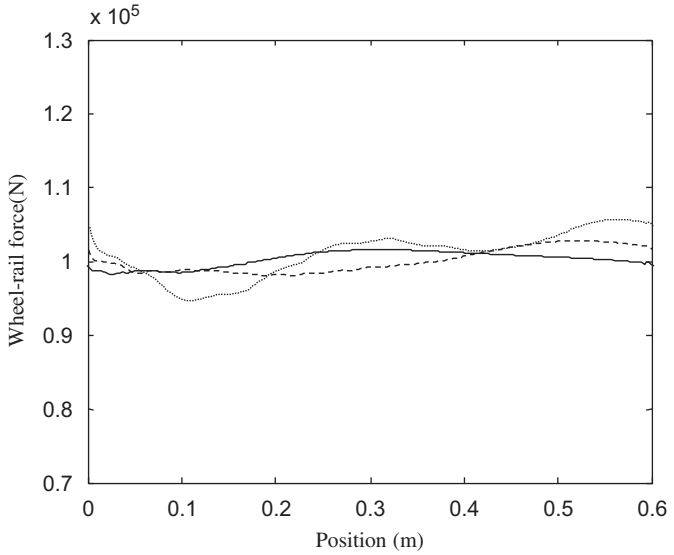

Fig. 5. Wheel–rail force position-history for the wheel moving at 20 m/s (———), 40 m/s (– – –) and 80 m/s (. . . . . .) over the rail with a smooth railhead.

Table 2
Ratios of the first three components of the wheel–rail force to the static load

Wheel speed (m/s)	First component (%)	Second component (%)	Third component (%)
20	1.4	0.4	0.0
40	2.0	0.6	0.4
60	2.0	2.1	0.4
80	3.4	2.3	0.4

Table 3
Wavelengths (m) and k, N and n in Eq. (8) of roughness at different excitation frequencies and wheel speeds

Excitation frequencies (Hz)	Wheel speed (20 m/s)	Wheel speed (40 m/s)	Wheel speed (80 m/s)
500	0.04 ($k = 15$, $N = 1$, $n = 0$)	0.08 ($k = 7$, $N = 2$, $n = 1$)	0.16 ($k = 3$, $N = 4$, $n = 3$)
1000	0.02 ($k = 30$, $N = 1$, $n = 0$)	0.04 ($k = 15$, $N = 1$, $n = 0$)	0.08 ($k = 7$, $N = 2$, $n = 1$)
2000	—	0.02 ($k = 30$, $N = 1$, $n = 0$)	0.04 ($k = 15$, $N = 1$, $n = 0$)

Fig. 9 shows that, at frequencies below the first pinned–pinned frequency, there is a correspondence between the peaks (dips) in this figure and the dips (peaks) in the receptance of the rail shown in Fig. 3. In other words, high stiffness of the rail leads to a high dynamic wheel–rail force component at the excitation frequency. The effect of the wheel speed is negligible except for frequencies within the ranges of 1000–1300 and 2500–3000 Hz. A strong influence of the wheel speed is seen in these two frequency ranges, particularly in the second one. These two frequency ranges correspond to the first (D in Fig. 3) and second (F in Fig. 3) pinned–pinned frequencies. These features distinguish the present approach from the moving roughness approach. If the moving roughness approach is employed, the dynamic wheel–rail force is just a pure harmonic at the roughness excitation frequency and it presents a peak at the first pinned–pinned frequency if the wheel is above a sleeper and a dip if the wheel is at the mid-span; and for frequencies higher than 2500 Hz, the magnitude of the wheel–rail force must be close to a constant, since for these frequencies the receptance of the contact spring is much higher than those of the track and the wheel.

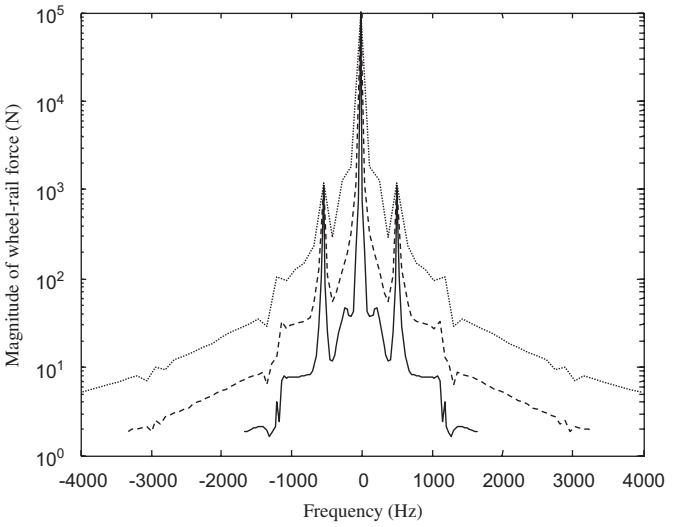

Fig. 6. Wheel–rail force spectrum for the wheel moving at 20 m/s (———), 40 m/s (– – –) and 80 m/s (. . . . . .) over the rail with a sinusoidal railhead of amplitude 10 μm at a wavelength corresponding to 500 Hz.

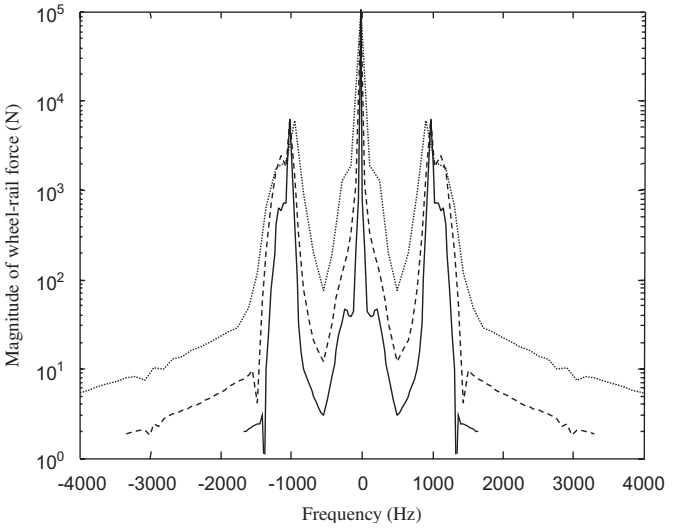

Fig. 7. Wheel–rail force spectrum for the wheel moving at 20 m/s (———), 40 m/s (– – –) and 80 m/s (. . . . . .) over the rail with a sinusoidal railhead of amplitude 10 μm at a wavelength corresponding to 1000 Hz.

The dynamic wheel–rail force position-history induced by the irregular rail profile only (the component due to the moving axle load excitation is subtracted from the total wheel–rail force) is shown in Fig. 10 for excitation frequency 1 kHz and Fig. 11 for 2 kHz. The histories are plotted for the same sleeper bay and the excitation frequency is fixed, so the roughness wavelength increases as the wheel speed increases. Fig. 10 shows that, since the excitation frequency is close to the first pinned–pinned frequency, the wheel–rail force history exhibits a complex pattern. As shown in Fig. 7, harmonic components of similar magnitudes exist around the excitation frequency and these harmonic components modulate each other, generating a complex resultant wheel–rail force history. A strong effect of the wheel speed is clearly revealed: the maximum wheel–rail force is shifted by the wheel speed from the sleeper towards the mid-span. However, since excitation frequency at 2 kHz is significantly different from the first and the second pinned–pinned frequencies, the dynamic

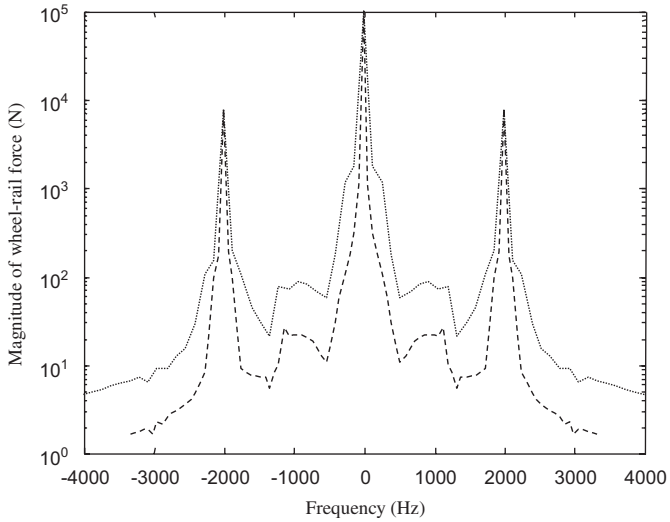

Fig. 8. Wheel–rail force spectrum for the wheel moving at 40 m/s (– – –) and 80 m/s (. . . . . .) over the rail with a sinusoidal railhead of amplitude 10 μm at a wavelength corresponding to 2000 Hz.

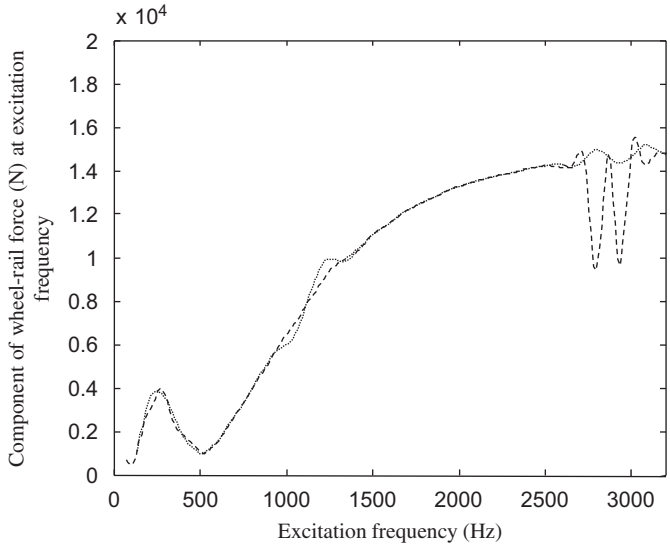

Fig. 9. The component of the wheel–rail force at the excitation frequency for the wheel moving at 40 m/s (– – –) and 80 m/s (. . . . . .) over the rail with a sinusoidal railhead of amplitude 10 μm.

wheel–rail force due to the rail irregularity is basically harmonic, following the pattern of the irregularity. This is confirmed by the wheel–rail force spectra shown in Fig. 8 in which a narrow and sharp peak occurs at the excitation frequency. The wheel speed does not have a significant effect at this frequency.

4.3. Wheel–rail force: four wheels moving along rail

Now discussion is turned to the case in which there are four wheels from the locomotive's two bogies moving along the rail, to investigate interactions between multiple wheels. The bogie wheelbase is 3.3 m long and the distance between the bogie centres is 10 m. In other words, the initial position of the four wheels are

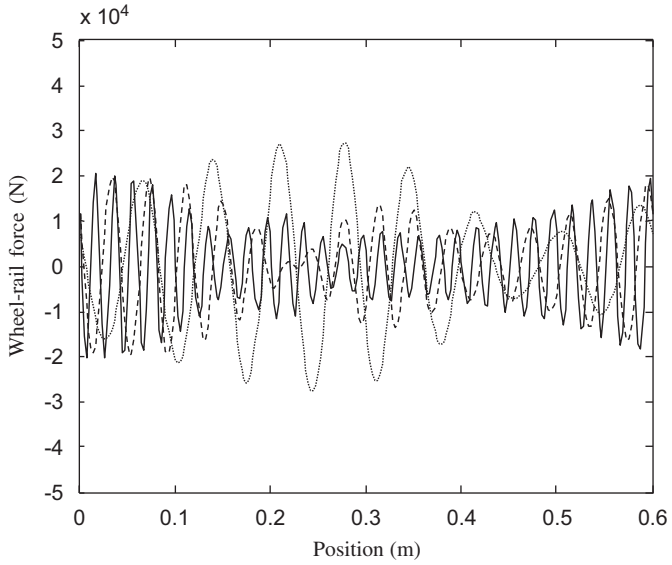

Fig. 10. Wheel–rail force position-history for the wheel moving at 20 m/s (———), 40 m/s (– – –) and 80 m/s (. . . . . .) over the rail with a sinusoidal railhead of amplitude 10 μm at a wavelength corresponding to 1000 Hz.

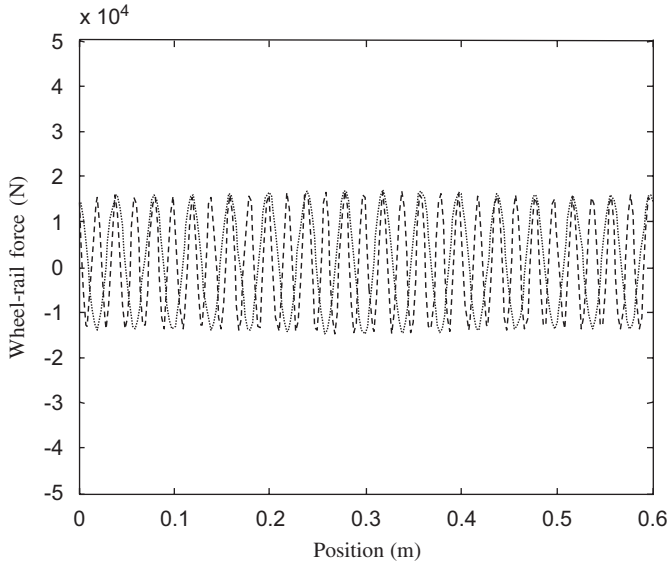

Fig. 11. Wheel–rail force position-history for the wheel moving at 40 m/s (– – –) and 80 m/s (. . . . . .) over the rail with a sinusoidal railhead of amplitude 10 μm at a wavelength corresponding to 2000 Hz.

$a_1 = 0$ m, $a_2 = -3.3$ m, $a_3 = -10$ m and $a_4 = -13.3$ m (see Eq. (14) and Fig. 1). The bogie wheelbase covers five and a half-sleeper bays.

As a wheel moves over a sleeper bay, dynamic stiffness provided by the rail to the wheel varies, due not only to the discrete rail supports, but also to the moving of other wheels. A moving static load produces to the rail mainly a moving deformation, which is not symmetric about the load: deformation behind the load is greater and extends to a larger distance than that ahead the load. This is particularly the case when the load speed is high. If the frequency is within the pass-band [11], a dynamic wheel–rail force generates rail vibration propagations ahead and behind the wheel, and the vibration wave behind the wheel is larger in both magnitude and wavelength than that ahead the wheel. Thus interactions between two adjacent moving wheels

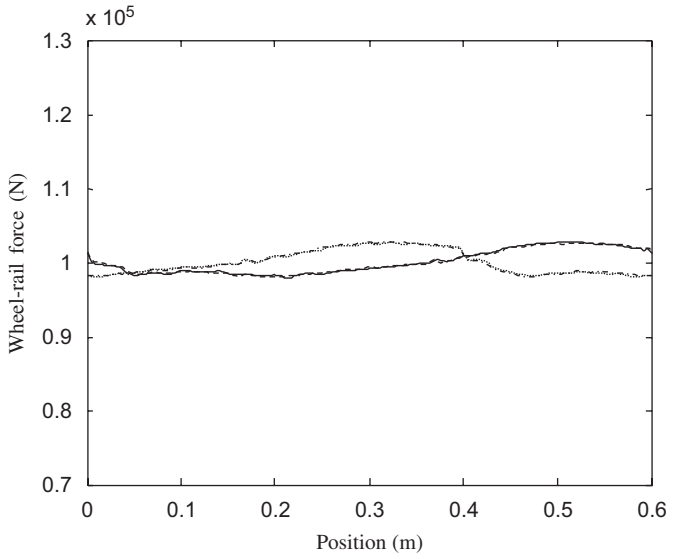

Fig. 12. Wheel–rail force position-history for the wheels moving at 40 m/s over the rail with a smooth railhead. ———, at the first wheel; – – –, at the second; – · –, at the third; . . . . . ., at the fourth.

are not symmetric: the effect received by the rear wheel from the front wheel is stronger than that received by the front wheel from the rear one.

4.3.1. Rail with a smooth railhead

For the rail with a smooth railhead, wheel–rail force position-histories of the four wheels are shown in Fig. 12 for the wheels moving at 40 m/s. They are wheel/rail forces for the wheels passing the same sleeper bay, termed the observation bay. Since the bogie wheelbase is relatively short, the wheel–rail forces within a bogie are indistinguishable. However, differences are clearly present between the two bogies due to the interactions between the wheels. Compared with Fig. 5 for a single wheel, the wheel–rail forces of the first bogie are almost identical to that of the single wheel. This indicates that the effects of the last two wheels on the first two wheel–rail forces are negligible.

4.3.2. Rail with a spatially harmonic railhead

Wheel–rail forces are also produced for the four wheels moving at 40 m/s over the rail with a spatially harmonic railhead of a single wavelength. The wheel–rail force component at the excitation frequency (*note*: roughness excitation frequencies have been chosen to equal the sleeper passing frequency and its multiples) is shown in Figs. 13–16 for the four wheels. At frequencies below 600 Hz, this component presents a small difference from that in the single wheel case shown in Fig. 8. In other words, for those frequencies, interacting effects on that wheel–rail force component (magnitude) are negligible. In fact, Fig. 2 of Ref. [11] shows that 230 to 520 Hz is a stop band. However, at higher frequencies, many strong peaks which are not found in Fig. 8 appear, showing strong interactions between the four wheels.

5. Conclusion

The Fourier-series approach is adopted and improved in this paper for calculating wheel–rail interactions generated by any number of wheels moving along a railway track which is represented by an infinitely long periodic structure. This approach assumes railhead roughness to be periodic in the track direction and the period is equal to the length of a number, N, of sleeper bays. By assuming linear dynamics for the wheel/track system and in the steady state, each wheel/rail force generated from roughness excitation as well as from the

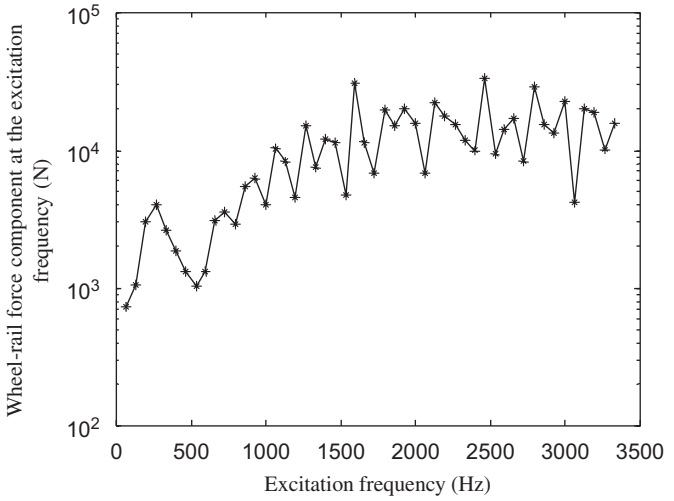

Fig. 13. Wheel–rail force component at the excitation frequency of the first wheel moving at 40 m/s over the rail with a sinusoidal railhead of amplitude 10 μm.

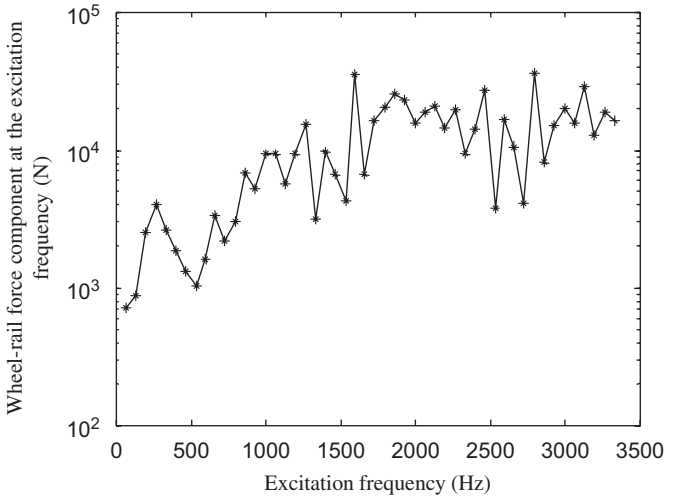

Fig. 14. Wheel–rail force component at the excitation frequency of the second wheel moving at 40 m/s over the rail with a sinusoidal railhead of amplitude 10 μm.

moving axle load excitation is shown to be a periodic function of time with the period being NL/c, where L is the sleeper spacing and c the wheel speed. With a special mathematical treatment, Fourier coefficients of the wheel/rail forces are shown to be determined by solving N uncoupled sets of linear algebraic equations. The coefficient matrix of each set of equations is independent of rail roughness and therefore this approach, combined with contact mechanics and wear process, is particularly useful in modelling the generation and growth of rail corrugation and roughness. By assuming a smooth railhead, the response of the wheel/track system to the moving axle load excitation is realised. Roughness equivalent to the moving axle load excitation is also defined. This equivalent roughness may, in addition to the actual rail roughness, be fed into a 'moving roughness' model in which the moving axle load excitation has not been taken into account, so that predictions from such a model can be improved. This equivalent roughness also provides a lower limit for rail roughness management. Conditions are also derived to ensure the existence and uniqueness of the above NL/c-periodic wheel/rail forces and at the same time forbid the existence of $2NL/c$, $3NL/c$, …-periodic wheel/rail forces.

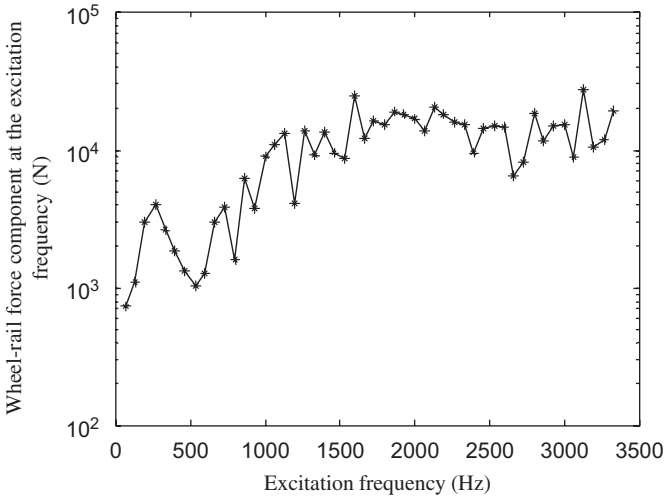

Fig. 15. Wheel–rail force component at the excitation frequency of the third wheel moving at 40 m/s over the rail with a sinusoidal railhead of amplitude 10 μm.

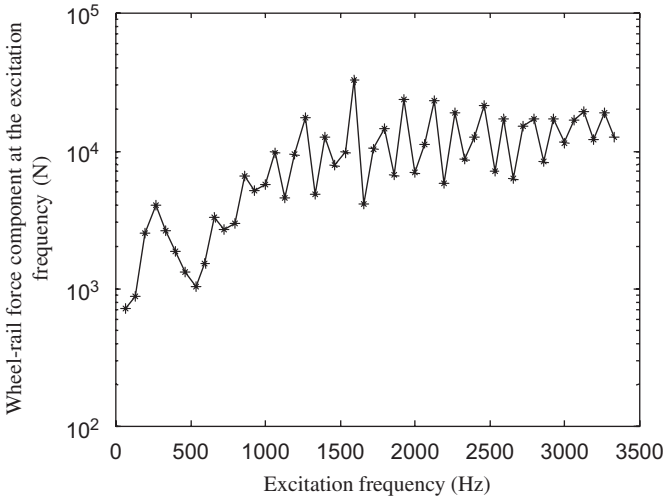

Fig. 16. Wheel–rail force component at the excitation frequency of the fourth wheel moving at 40 m/s (– – –) over the rail with a sinusoidal railhead of amplitude 10 μm.

Based on calculations using time-domain models, this periodic solution is believed to be asymptotically stable under conventional conditions, although a rigorous proof is desirable.

Results are produced for a single locomotive wheel and for four such wheels running at different speeds over a conventional ballasted track with either a smooth railhead or a rough railhead of different wavelengths. It is demonstrated that, for the purpose of rolling noise prediction, roughness levels equivalent to the moving axle load excitation can be approximated to be independent of wheel speed. Opposite to that, all the dynamic wheel–rail force components due to the moving axle excitation increase with the wheel speed. Dynamic wheel–rail forces due to the moving axle load excitation consist of harmonic components at the sleeper-passing frequency and its multiples. The component at the sleeper passing frequency is dominant if the wheel speed is low. However, at high wheel speeds, the second component at twice the sleeper-passing frequency can be as strong as the first. A broad peak is present in the wheel–rail force spectrum at the first pinned–pinned frequency.

When the roughness excitation is much higher than the moving axle load excitation and the excitation frequency is significantly different from the first and second pinned–pinned frequencies of the track, the wheel speed has an insignificant effect on the wheel–rail force component at that frequency, and even on the total wheel–rail force. The wheel–rail force position-history exhibits a harmonic wave pattern. However, around the pinned–pinned frequencies, the role of the wheel speed cannot be neglected, even for roughness excitation alone. The wheel–rail force position-history displays a complex waveform due to modulations of components of similar magnitudes and frequencies.

Strong interactions between multiple wheels are demonstrated at frequencies above 600 Hz for the chosen track and bogies.

Acknowledgements

Part of the material in this paper is from the work supported by the EPSRC and Rail Research UK under project A3: *Railway noise: curve squeal, roughness growth, friction and wear*.

Thanks to Dr. G. Xie, Rail Technology Unit, Manchester Metropolitan University and Dr. B. Croft, ISVR, University of Southampton, for the comparison with their time-domain wheel/rail interaction models.

References

[1] P.J. Remington, Wheel/rail rolling noise—part I: theoretical analysis, *Journal of Acoustical Society of America* 81 (1987) 1805–1823.
[2] P.J. Remington, Wheel/rail rolling noise—part II: validation of the theory, *Journal of Acoustical Society of America* 81 (1987) 1824–1832.
[3] D.J. Thompson, B. Hemsworth, N. Vincent, Experimental validation of the TWINS prediction program for rolling noise—part I: description of the model and method, *Journal of Sound and Vibration* 193 (1996) 123–135.
[4] D.J. Thompson, P. Fodiman, H. Mahé, Experimental validation of the TWINS prediction program for rolling noise—part II: results, *Journal of Sound and Vibration* 193 (1996) 137–147.
[5] S. Müller, A linear wheel–track model to predict instability and short pitch corrugation, *Journal of Sound and Vibration* 227 (1999) 899–913.
[6] K. Knothe, Chapter 4: on non-steady state rolling contact and corrugations, *Rolling Contact Phenomena. CISME Courses and Lectures*, No. 411, Springer, New York, 2000.
[7] A. Valdivia, Interaction Between High-frequency Wheel–Rail Dynamics and Irregular Rail Wear—A Linear Model, PhD Thesis, TU Berlin, 1987.
[8] K. Hempelmann, K. Knothe, An extended linear model for the prediction of short-pitch corrugation, *Wear* 191 (1996) 161–169.
[9] C.O. Frederick, A rail corrugation theory, *Proceedings of the Second Conference on the Contact Mechanics and Wear of Rail/Wheel Systems*, 1986.
[10] A. Igeland, Railhead corrugation growth explained by dynamic interaction between track and bogie wheelsets, *Proceedings of the Institution of Mechanical Engineers, Part F: Journal of Rail and Rapid Transit* 210 (1996) 11–20.
[11] X. Sheng, M. Li, Propagation constants of railway tracks as a periodic structure, *Journal of Sound and Vibration* 299 (2007) 1114–1123.
[12] X. Jin, Z. Wen, K. Wang, Effect of track irregularities on initiation and evolution of rail corrugation, *Journal of Sound and Vibration* 285 (2005) 121–148.
[13] A. Nordborg, Wheel/rail noise generation due to nonlinear effects and parametric excitation, *Journal of Acoustical Society of America* 111 (2002) 1772–1781.
[14] T.X. Wu, D.J. Thompson, On the parametric excitation of wheel/track system, *Journal of Sound and Vibration* 278 (2004) 725–747.
[15] X. Sheng, C.J.C. Jones, D.J. Thompson, Responses of infinite periodic structures to moving or stationary harmonic loads, *Journal of Sound and Vibration* 282 (2004) 125–149.
[16] X. Sheng, C.J.C. Jones, D.J. Thompson, *Interactions Between Multiple Moving Wheels and a Railway Track*, University of Southampton, Institute of Sound and Vibration Research, Technical Memorandum No. 930, 2004.
[17] X. Sheng, C.J.C. Jones, D.J. Thompson, et al., Simulation of roughness initiation and growth on railway rails, *Journal of Sound and Vibration* 293 (2006) 819–829.
[18] H. Kruse, K. Popp, A modular algorithm for linear, periodic train–track models, *Archive of Applied Mechanics* 71 (2001) 473–486.
[19] P.M. Belotserkovskii, The steady vibrations and resistance of a railway track to uniform motion of unbalanced wheel, *Journal of Applied Mathematics and Mechanics* 67 (2003) 763–773.
[20] P.M. Belotserkovskii, The interaction of an infinite wheel–train with a constant spacing between the wheels moving uniformly over a rail track, *Journal of Applied Mathematics and Mechanics* 68 (2004) 923–931.

[21] S.N. Verichev, A.V. Metrikine, Instability of vibrations of a mass that moves uniformly along a beam on a periodically inhomogeneous foundation, *Journal of Sound and Vibration* 260 (2003) 901–925.
[22] R.A.J. Ford, D.J. Thompson, Simplified contact filters in wheel/rail noise prediction, *Journal of Sound and Vibration* 293 (2006) 807–818.
[23] A.V. Metrikine, K. Popp, Vibration of a periodically supported beam on an elastic half-space, *European Journal of Mechanics A/Solids* 18 (1999) 679–701.